Dynamic Influences on a High-Affinity, High-Specificity Interaction Involving the C-Terminal SH3 Domain of p67^{phox}†

Kaushik Dutta,‡ Huanhuan Shi,§ Eduardo R. Cruz-Chu,§ Keiichiro Kami,|| and Ranajeet Ghose§,⊥,*

The New York Structural Biology Center, New York, New York 10031, Department of Chemistry, City College of the City University of New York, New York 10031, Department of Biochemistry and Molecular Biology, Medical Institute of Bioregulation, Kyushu University, Fukuoka, 812-8582, Japan, and Graduate Center of the City University of New York, New York, New York 10016

Received December 30, 2003; Revised Manuscript Received March 29, 2004

ABSTRACT: An analysis of the backbone dynamics of the C-terminal Src homology 3 (SH3) domain of p67^{phox}, p67^{phox}SH3(C), in complex with a 32-residue high-affinity (K_d = 24 nM) peptide, Pf, from the C-terminal region of p47^{phox} is presented. This paper represents the first detailed analysis of the backbone dynamics and the ligand-induced changes therein of a high-affinity, high-specificity interaction involving an SH3 domain. The dynamic features are compared with those in the high-affinity, highly specific interaction between the SH3 domain of C-terminal Src kinase (Csk-SH3) and a proline-rich peptide from proline-enriched phosphatase (PEP). Both systems share common dynamic features especially in the canonical PxxP motif recognition surface where slow micro- to millisecond time scale dynamics persist on complex formation especially in several residues that are implicated in ligand recognition and in stabilizing the SH3 fold. These residues are highly conserved in SH3 domains. Ile505, which lies outside the PxxP recognition motif on p67^{phox}SH3(C) and is key in conferring high specificity to the p67^{phox}SH3(C)/Pf interaction, becomes more disordered upon complex formation. This behavior is similar to that seen in the residues that constitute the specificity surface in Csk-SH3.

The Src homology 3 (SH3)[1] domain is a small (60−70 residues) noncatalytic, structural motif (*1*, *2*) that is ubiquitous in eukaryotic cells. Over 500 SH3 domains have been identified in the human genome. Several key intracellular signal transduction pathways involve interactions mediated by SH3 domains (*2*−*4*). It has long been recognized that SH3 domains bind proline-rich ligands containing the consensus PxxP ("x" is any amino acid) sequence (*5*) with low affinity ($K_d \approx 10-50\ \mu$M) in a nonspecific fashion (*2*). The PxxP motif forms a canonical type II polyproline helix with two possible helical orientations depending on the N- (class I) or C-terminal (class II) location of a flanking Arg (or Lys) residue (R/KxxPxxP for class I and PxxPxR/K for class II ligands) (*6*). However, the search for specificity in interactions involving SH3 domains in vivo has been an elusive one. It was recently shown that the nonreceptor tyrosine kinase C-terminal Src kinase (Csk), through its SH3 domain, takes part in a high-affinity (0.8 μM), highly specific interaction with the proline-enriched phosphatase, PEP (*7*) in hematopoietic cells. This interaction helps localize PEP near active c-Src, which is then phosphorylated on a key C-terminal tyrosine residue by Csk and dephosphorylated on a tyrosine residue in the so-called "activation loop" in its catalytic domain by PEP. These two actions together take c-Src from the active, transforming state to an inactive state (*8*, *9*). A high-resolution solution structure of the SH3 domain of Csk (Csk-SH3) complexed with a peptide (PEP-3BP1) encompassing the key residues that constitute the SH3-binding region from PEP revealed that the source of specificity lay outside the PxxP recognition motif (*10*) and consisted of a hydrophobic interaction involving two residues (Ala40 and Thr42) on Csk-SH3 and two residues Ile625′ (ligand residues are primed from hereon) and Val626′ (both C-terminal to the PxxP sequence) on PEP.

This paper was followed by the discovery of another natural, highly specific interaction involving an SH3 domain between two cytosolic components of the NADPH oxidase complex (*11*). The NADPH oxidase complex plays a major role in the phagocytic defense mechanism against microbial pathogens through the production of superoxide anions leading to the generation of reactive oxygen species. It was shown that the C-terminal SH3 domain of p67^{phox} [henceforth referred to as p67^{phox}SH3(C)] binds a proline-rich segment from the C terminus of p47^{phox}. This interaction has the

† This work has been supported in part by a grant from the RCMI initiative of the National Institutes of Health at the City College of New York, by an NSF−CAREER award (MCB-0347100) to R.G., and support from the Graduate Research and Teaching Initiative of the State of New York. We also acknowledge the National Institutes of Health for instrumentation support (P41 GM-66354) to the New York Structural Biology Center. K.D. was supported on a grant (RO1 GM-47021) from the National Institutes of Health.

* To whom correspondence should be addressed: Department of Chemistry, City College of the City University of New York, 138th Street and Convent Avenue, New York, NY 10031. Phone: (212) 650-6049. Fax: (212) 650-6107. E-mail: rghose@sci.ccny.cuny.edu.

‡ The New York Structural Biology Center.

§ City College of the City University of New York.

|| Kyushu University.

⊥ Graduate Center of the City University of New York.

[1] Abbreviations: CPMG, Carr−Purcell−Meiboom−Gill; DTT, dithiothreitol; MOPSO, 3-[*N*-morpholino]-2-hydroxypropanesulfonic acid; NMR, nuclear magnetic resonance; SH3, Src homology 3.

10.1021/bi030268d CCC: $27.50
Published on Web 06/03/2004

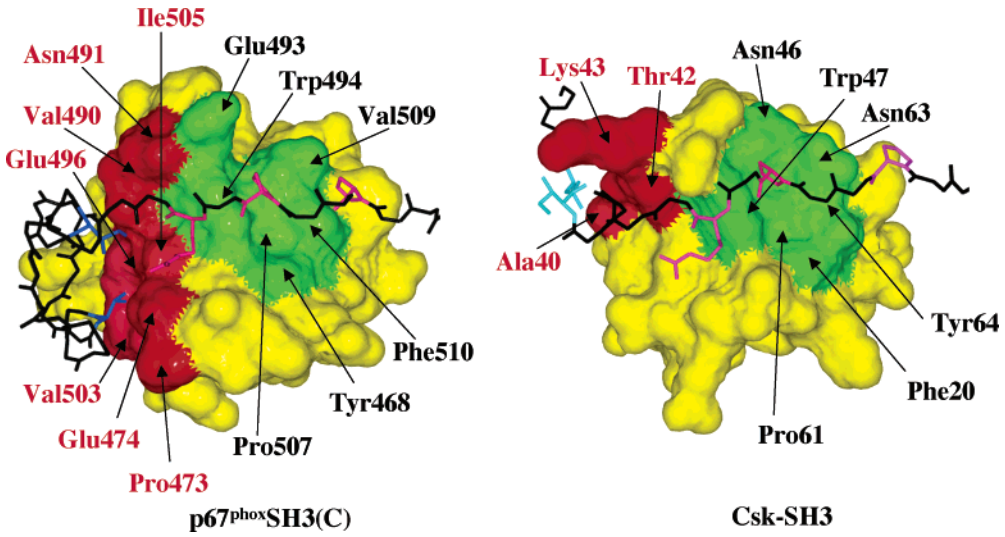

FIGURE 1: Comparison of the ligand interaction surfaces (see text) for the p67^{phox}SH3(C)/Pf (left) and Csk-SH3/PEP-3BP1 (right) complexes. The proline-helix recognition surface is shown in green and the specificity surface, in red. Key Arg residues (Arg368′ in Pf and Arg619′ in PEP-3BP1) and Pro residues (Pro363′ and Pro366′ in Pf and Pro614′ and Pro617′ in PEP-3BP1) are shown in pink. Ile374′ and Thr382′ responsible for specific interactions in Pf are shown in dark blue, while Ile625′ and Val626′ on PEP-3BP1 are shown in cyan. Residues that recognize the canonical PxxPxR motif are labeled in black (and the order of the corresponding residues is followed in the labeling scheme; e.g., Trp494 on p67^{phox}SH3(C) corresponds to Trp47 on Csk-SH3 etc.). Residues that form the specificity surface in each case are labeled in red.

highest measured affinity for a natural SH3/peptide interaction (K_d = 24 nM) (*11*), where a canonical PxxP motif is involved. The determinant of the specificity of this interaction, as in the case of the Csk−PEP interaction, was outside the PxxP region and involved the recognition of a C-terminal extension of the PxxP sequence (*11*) and consisted of two key hydrophobic residues Ile374′ and Thr382′. Both the C-terminal extension, excluding the PxxP motif and the PxxP motif itself, were shown to individually bind p67^{phox}SH3(C), albeit with lesser affinity than the full construct. This observation has provided momentum to the belief that specific interactions involving SH3 domains involve sequences different from the conventional PxxP motif and the affinity of the interaction is governed by the cooperative recognition of the PxxP motif and the specificity motif (*2*, *12*). A comparison between the PxxP-recognition (green) and "specificity" (red) motifs in p67^{phox}SH3(C) and Csk-SH3 is shown in Figure 1. It is notable that the general shape and position of the PxxP-recognition surfaces are similar in both cases, while the specificity surfaces are quite different.

Several authors have studied the dynamic properties of the proline-helix recognition surface in SH3 domains and the changes thereof on complex formation (*13*, *14*). However, very little is known on the dynamic behavior of the specificity surface (*10*). Recent NMR relaxation measurements on the Csk-SH3 backbone revealed clues into interesting dynamical properties of the specificity surface. It was seen that the two residues on Csk-SH3, namely, Ala40 and Thr42, that were involved in a highly specific interaction with Val626′ on PEP showed extensive disorder in their backbone region. The backbone amide vectors on all three residues displayed order parameter (S^2) values that were far lower than the mean value for the backbone residues, whereas interactions between the corresponding methyl groups (Cβ on Ala40, Cγ_2 on Thr42, and Cγ_2 on Val626′) were key in determining the specificity of the Csk−PEP interaction. It was also seen that several key residues comprising the proline-helix recognition surface were dynamic on the micro- to millisecond time scale, indicating large amplitude collective motions. On the other hand, none of the residues that comprised the specificity surface exhibited motion on the micro- to millisecond time scale (*10*). This indicated a possible correlation between the nature of the dynamics exhibited by each surface and the nature of their contribution toward ligand recognition. Such correlations between details of the dynamic properties and the affinity and specificity of ligand recognition have been inferred in several other systems (*15*, *16*). However, free Csk-SH3 exists as a dimer of dimers in solution, making a detailed investigation of the dynamics of the free and complexed states difficult. This problem is further complicated by the fact that the oligomerization surface occludes the ligand recognition surfaces and any mutations to prevent oligomerization would necessarily affect ligand binding. However, the free p67^{phox}SH3(C), can be obtained in a well-defined monomeric state in solution. Thus, the p67^{phox}SH3(C)/p47^{phox}-Pf system provides the unique opportunity to study the detailed dynamic properties of the individual ligand recognition surfaces (PxxP recognition and specificity), the changes thereof on complex formation and the extent of dynamic coupling between the two surfaces. We present here the first detailed investigation of the backbone dynamics of a high-affinity interaction involving an SH3 domain.

MATERIALS AND METHODS

Sample Preparation. ^{15}N-labeled constructs of p67^{phox}SH3(C) (455−516) and the p47^{phox} tail peptide (Pf) consisting of residues 360′−390′ were purified as detailed previously (*11*). In the case of the complex, a double mutant of p67^{phox}-SH3(C) (C499S and C514S) was used as in Kami et al. (*11*). In the case of free p67^{phox}SH3(C), both the double mutant and wild type exist in an equilibrium between folded and unfolded states, complicating the analysis of the measured relaxation rates. This equilibrium is shifted in favor of the folded state at high salt concentrations (~500 mM Na_2SO_4). However, the double-mutant had a detectable percentage of

the unfolded state even at high salt concentrations, while the wild type was determined to be in a single, well-defined, monomeric, folded state. Thus, relaxation data were acquired for the wild-type free p67^{phox}SH3(C). It was not expected that this double mutation would result in any significant structural perturbation in the SH3-fold or affect the interpretation of the backbone dynamics and the changes because of protein−peptide interactions (see the Results).

In the case of the complex, the NMR sample contained 0.8 mM ^{15}N-labeled p67^{phox}SH3(C) with 15% molar excess of the p47^{phox} tail peptide Pf, 5 mM MOPSO, 30 mM DTT, 100 mM KCl, trace quantities of NaN_3, and 15% D_2O, and the pH was adjusted to 7.1. In the case of free p67^{phox}SH3-(C) (0.6 mM), the sample buffer was the same as above and also contained 500 mM of Na_2SO_4 to stabilize the folded state.

Quantitative Measure of Protein−Peptide Contacts. To analyze the backbone amide ^{15}N relaxation rates of free p67^{phox}SH3(C) and the changes thereof upon complex formation with the tail peptide (Pf) from p47^{phox} and relate these changes to the formation of protein−peptide contacts, it was important to find a simple measure on a per residue basis characterizing these contacts. Thus, to find a numerical characteristic of the residues on p67^{phox}SH3(C), which were in close contact with the peptide Pf, we defined a normalized contact factor Λ given by

$$\Lambda_i = \frac{\sum_j \sum_k (5 - d_{jk}^i)}{\max|\Lambda|} \quad (1)$$

where Λ_i is the normalized contact factor for the ith residue, d_{jk}^i is the distance, in angstroms of the jth proton on residue i of the SH3 domain with the kth proton on the ligand. A cutoff distance of 5 Å was used. Note that the closer the jth and kth protons, the larger the value within the summation, and larger the number of intermolecular contacts, the larger is the value of Λ_i ($0 \leq \Lambda_i \leq 1$). We also defined a scaled chemical shift change (Δ_i) upon complex formation. This is given by

$$\Delta_i = \sqrt{[\delta_{H,i}^{free} - \delta_{H,i}^{complex}]^2 + [(\gamma_N/\gamma_H)(\delta_{N,i}^{free} - \delta_{N,i}^{complex})]^2} \quad (2)$$

$\delta_{H,i}^{free}$, $\delta_{H,i}^{complex}$, $\delta_{N,i}^{free}$, and $\delta_{N,i}^{complex}$ are the chemical shifts of the free and complexed p67^{phox}SH3(C) for the amide $^1H^N$ and ^{15}N nuclei of the ith residue. γ_H and γ_N are the gyromagnetic ratios for ^{1}H and ^{15}N nuclei.

NMR Spectroscopy and Data Processing. All NMR experiments were performed using either a Varian Inova spectrometer operating at ^{1}H frequency of 600 MHz or Bruker Avance spectrometers (equipped with CryoProbes) operating at ^{1}H frequencies of 600 and 800 MHz. All spectrometers were equipped with triple-resonance probes capable of applying pulsed field gradients along the z axis. All experiments were performed at 25 °C.

A complete set of R_1, R_2, and {^{15}N-$^1H^N$}-NOE measurements (*17*) were made at 600 MHz, and additional R_1 and R_2 measurements were made at 800 MHz for p67^{phox}SH3-(C) in the free and complexed states. Recycle delays of 1.5 s were used in the R_1 and R_2 relaxation measurements for both free and complexed forms. The following relaxation delays were used to measure the R_2 values at 600 MHz, free: 10, 30 (×2), 70, 90, 110, 130, and 150 ms; 600 MHz, complex: 10, 30, 50 (×2), 70 (×2), 90, 110, 130, 150, and 200 ms; 800 MHz, free: 4 (×2), 12, 22, 32, 42, 72, 102 (×2), and 148 ms; and 800 MHz, complex: 4, 6, 14, 22, 26 (×2), 62, 66 (×2), 78, 90 ms. For the R_1 measurements, the following variable relaxation delays were used at 600 MHz, free: 10, 50 (×2), 90, 170, 330, 510 (×2), and 750 ms; 600 MHz complex: 10 (×2), 150, 300, 400, 500, 700, 850 × 2, and 1000 ms; 800 MHz, free: 10, 40 (×2), 80, 160, 320, 500 (×2), and 750 ms; and 800 MHz, complex: 10, 150, 300, 400 (×2), 700, 850, and 1000 (×2) ms.

$R_{1\rho}$ values were obtained at 600 MHz for the free and complexed forms using the following variable relaxation delays: free, 10, 30, 50, 70, 90, 110 (×2), 130, 150, and 200 ms and complex, 10, 30, 50 (×2), 70 (×2), 90, 110, 130, 150, and 200 ms. A spin-lock field ($\Delta\omega_{SL}$) of 1500 Hz was used to obtain sample heating effects similar to those in the R_2 measurements above to allow an accurate comparison between the two rates. A recycle delay of 1.5 s was used in all cases. The measured $R_{1\rho}^{app}$ were corrected for off-resonance effects using the following equation

$$R_{1\rho} = \frac{R_{1\rho}^{app} - R_1 \cos^2\beta}{\sin^2\beta} \quad (3)$$

with $\beta = \tan^{-1}(\omega_{SL}/\Delta\omega)$ and $\Delta\omega$ is the offset from the carrier.

Relaxation-compensated CPMG experiments (RC-CPMG) (*18*) were performed on both the free and the complexed forms to determine R_{av} values (average of the inphase, $N_{\pm}$, and antiphase, $2N_{\pm}H_z$, decay rates), with $\tau_{CP} = 1$ ms (τ_{CP} is the delay between the 180° pulses of the CPMG cycle) using relaxation delays of 0 (×2), 8, 16, 32, 48, 80, 112, and 148 ms and $\tau_{CP} = 10$ ms using relaxation delays of 0 (×2), 40, 80, 120 (×2), 160, and 200 ms. Recycle delays of 1.5 s were used in all cases.

All data were processed using the nmrPipe (*19*) software suite and visualized with NMRdraw (*19*) and NMRView (Bruce Johnson, Merck Research Laboratories). Peak intensities were measured with NMRview with random errors being estimated from duplicate spectra. The relaxation rates R_1, $R_{1\rho}$, R_2, and R_{av} were determined by fitting the peak intensity $I(t)$ to a single-exponential function given by $I(t) = I_0\, e^{-Rt}$ ($R = R_1$, $R_{1\rho}$, R_2, and R_{av}) using CURVEFIT (A. G. Palmer, III, Columbia University).

Steady-state {^{15}N-$^1H^N$}-NOE values were obtained by recording two spectra with and without a 3.0 s period of proton saturation. The error (σ_{NOE}) was determined using the following equation

$$\sigma_{NOE} = \frac{I_{sat}}{I_{unsat}}\left(\left(\frac{\sigma_{sat}}{I_{sat}}\right)^2 + \left(\frac{\sigma_{unsat}}{I_{unsat}}\right)^2\right)^{1/2} \quad (4)$$

where I_{sat} and I_{unsat} represent the measured intensities of a particular resonance in the presence and absence of proton saturation, and σ_{sat} and σ_{unsat} represent the root-mean-square variation in the noise in empty spectral regions of the spectra with and without proton saturation.

Analysis of the Hydrodynamic Properties. The hydrodynamic properties of the free and complexed forms of p67^{phox}-

SH3(C) were determined using DIFFTENS2.0 (*20*) that utilizes methods described previously (*20*). To determine which residues were in exchange, the conventional R_2/R_1 ratio was not used. Instead, we defined a quantity J_{prod} given by

$$J_{prod} = J'(0)\, J'(0.87\omega_H) = \frac{S^4 \tau_{c,eff}{}^2}{1 + (0.87\omega_H \tau_{c,eff})^2} \quad (5)$$

where $\tau_{c,eff}$ is an effective correlation time and may be related to the effective diffusion constant D_{eff} ($\tau_{c,eff} = 1/6D_{eff}$) defined by Ghose et al. (*20*), and the reduced spectral density functions $J'(\omega)$ are given by

$$J'(0) = \frac{2R'_2 - R'_1}{4(c^2 + d^2)}$$

$$d^2 J'(0.87\omega_H) = HF \quad (6)$$

with (*20*)

$$R'_1 = R_1 - 7\left(\frac{0.921}{0.87}\right)^2 HF$$

$$R'_2 = R_2 - \frac{13}{2}\left(\frac{0.955}{0.87}\right)^2 HF$$

$$HF = -\frac{\gamma_N}{5\gamma_H}(1 - NOE)R_1 \quad (7)$$

$c = \gamma_N B_0 \Delta\sigma/3$; $d = -(\mu_0/4\pi)(\gamma_H \gamma_N \hbar/2r_{NH}{}^3)$, where the symbols have their usual meaning. Values of $r_{NH} = 1.02$ Å and $\Delta\sigma = -160$ ppm were used. In the limit of slow overall tumbling, when $(0.87\omega_H)^2 \tau_{c,eff}{}^2 \gg 1$, the dependence of J_{prod} on the correlation time vanishes, making it less susceptible to local rotational anisotropy effects than the conventional R_2/R_1 approach. Exchange effects only serve to increase the value of J_{prod} (by increasing $J'(0)$ values) above the mean, while small S^2 values tend to decrease it. Thus, using this approach, those residues that satisfy the following eq 8 below were considered to be in exchange where the mean and

$$J_{prod,i} > \langle J_{prod} \rangle + 1.5\Delta J_{prod} \quad (8)$$

standard deviation $\langle J_{prod} \rangle$ and ΔJ_{prod} were recalculated by excluding the residues that satisfied eq 8. This approach is similar to that suggested by Kneller et al. (*21*).

Errors (68.3% confidence limits) in the principal values and orientation of the rotational diffusion tensor were obtained from the analytically determined inverse covariance matrix of the fits. Model selection between the fully anisotropic, axially symmetric, and isotropic models was performed using the statistical *F* test. Probabilities (*P*, %), indicating the possibility that the improvement in fits on increasing model complexity were obtained by chance, were calculated for each of the pairs of models, fully anisotropic/axially symmetric and axially symmetric/isotropic. Values of $P > 5\%$ were not considered to be statistically significant.

Lipari−Szabo Model-Free Analysis. An analysis of the microdynamic motional parameters using the Lipari−Szabo formalism (*22*) was performed utilizing DYNAMICS (*23*) using the R_1, R_2, and $\{^{15}N\text{-}^1H^N\}$-NOE data at 600 MHz in combination with R_1 and R_2 data at 800 MHz. Several runs

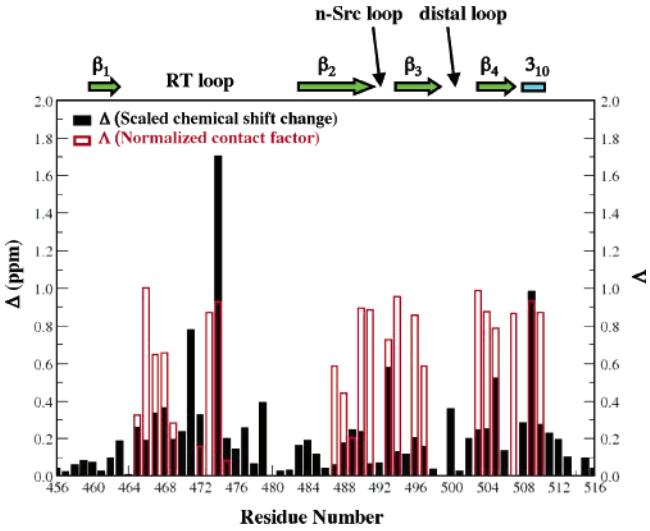

FIGURE 2: Plots of the normalized chemical-shift changes (△, black) between free p67^{phox}SH3(C) and that complexed with the tail peptide (Pf) from p47^{phox}. Also shown are the normalized contact factors (Λ, red) between p67^{phox}SH3(C) and Pf.

were carried out using various subsets of the relaxation rates to determine the stability of the analysis, the robustness of the selected models, and estimated microdynamic parameters with respect to completeness of the datasets. Errors (68.3% confidence limits) in the microdynamic parameters were obtained from the analytic inverse covariance matrixes of the fits. This method of error estimation is crucial because it takes into account both the random errors as well as the model selection errors. The latter may be, by far, the most dominant in highly nonlinear multiparameter fits such as in the present case. Commonly used Monte Carlo based approaches estimate only the random errors because of noise in the experimental data. The microdynamic parameters (including the overall correlation time, τ_c, obtained from the hydrodynamic analysis described above) were optimized by minimizing the χ^2 value determined by eq 9 below The

$$\chi^2 = \sum_j \sum_f \sum_r \left(\frac{X_{j,f,r}{}^{obs} - X_{j,f,r}{}^{calc}}{\sigma_{j,f,r}{}^{800}} \right)^2 \quad (9)$$

summation is over the measured relaxation rates X_i (R_1, R_2, and $\{^{15}N\text{-}^1H^N\}$-NOE or a subset thereof), the two fields *f* (600 MHz and 800 MHz), and over the residues *r* (456−516). Models used and computational strategies employed have been discussed at length previously (*23*). The dynamics of 10 residues were not interpreted in detail and are excluded from the discussion below. These include three residues (456, 457, and 458) at the extreme N terminus, two at the extreme C terminus (515 and 516), and the residues including, immediately preceding, and following the C499S and C514S mutations (498, 499, 500, 513, and 514).

RESULTS

Relaxation Measurements of Amide ^{15}N. Figure 2 shows the normalized contact factors Λ_i defined in eq 1 (red) plotted against the residue number to indicate regions of protein−peptide contacts. Also shown for comparison are the scaled chemical-shift changes Δ_i defined in eq 2 (black). Key elements of secondary structure characteristic to the

Table 1: Summary of the Measured Relaxation Rates for Free p67^{phox}SH3(C) and the p67^{phox}SH3(C)/Pf Complex[a]

species	R_1(600)	R_1(800)	R_2(600)	R_2(800)	$R_{1\rho}$(600)[b]	NOE(600)
free	2.35 ± 0.47	1.66 ± 0.25	6.93 ± 2.09	7.39 ± 2.59	7.10 ± 2.90	0.70 ± 0.25
complex	1.66 ± 0.13	1.25 ± 0.13	9.99 ± 1.85	11.35 ± 2.43	10.03 ± 1.53	0.71 ± 0.22

[a] All rates (where applicable) are in units of sec^{-1}. [b] $R_{1\rho}$ values are corrected for off-resonance effects using eq 3.

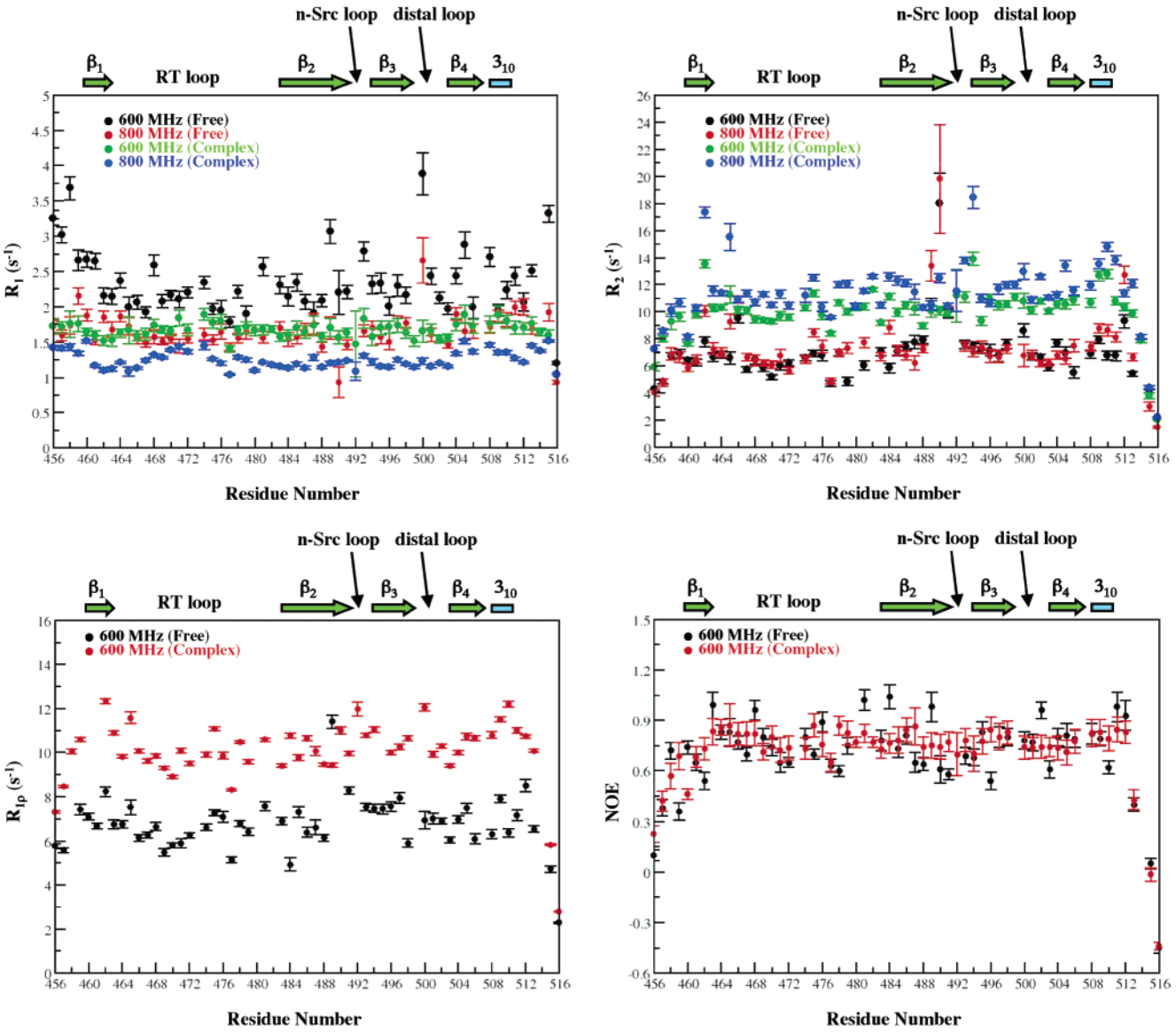

FIGURE 3: (a) Plots of R_1 (s^{-1}) of the free p67^{phox}SH3(C) at 600 MHz (black) and 800 MHz (red) and the p67^{phox}SH3(C)/Pf complex at 600 MHz (green) and 800 MHz (blue). (b) Plots of R_2 (s^{-1}) of the free p67^{phox}SH3(C) at 600 MHz (black) and 800 MHz (red) and the p67^{phox}SH3(C)/Pf complex at 600 MHz (green) and 800 MHz (blue). (c) Plots of $R_{1\rho}$ (s^{-1}) of the free p67^{phox}SH3(C) (black) and the p67^{phox}SH3(C)/Pf complex (red) at 600 MHz. (d) Plots of {^{15}N-^{1}H^{N}}-NOE of the free p67^{phox}SH3(C) (black) and the p67^{phox}SH3(C)/Pf complex (red) at 600 MHz.

SH3 domain fold family are indicated. Δ_i values for the proline residues 473 and 507 and the residues 499 and 514 (corresponding to the Cys to Ser mutations) are not reported.

Next, it was necessary to determine whether the different buffers (high salt for free and low salt for complex) would affect the interpretation of the microdynamic parameters. The HSQC spectra (not shown) for the complex both in high- and low-salt conditions are identical. Further, R_2 values measured at 600 MHz for the complex under high- and low-salt conditions showed a correlation of 0.99, with the values at high salt being slightly higher corresponding to a change in viscosity and the resultant increase in τ_c. A comparison of the HSQC spectra (not shown) for the free mutant and wild-type p67^{phox}SH3(C) at high salt reveals differences near the site of the mutation, at the end of the RT loop, and at the extreme N and C termini. However, the mutations showed no significant perturbations in the resonance positions of any of the residues involved in ligand recognition. A comparison of the R_2 values of the wild-type and mutant p67^{phox}SH3(C) reveals a correlation of 0.93. Residues at the extreme N and C termini and near the site of the mutation (see below) were excluded in the detailed analysis of the relaxation rates.

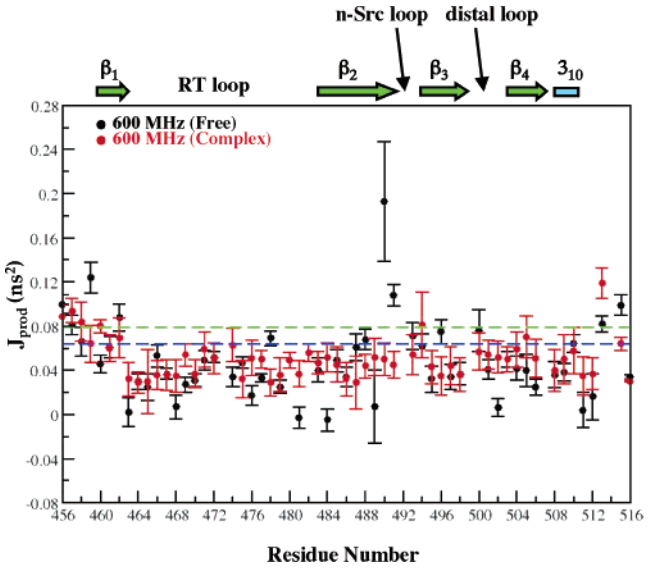

FIGURE 4: Plot of $J_{prod} = J'(0)\ J'(0.87\omega_H)$ for free p67^{phox}SH3(C) (black) and the p67^{phox}SH3(C)/Pf complex (red), and the dotted lines (green and blue = free and complexed, respectively) depict the mean value, $\langle J_{prod}\rangle + 1.5 \times$ the standard deviation (ΔJ_{prod}). Values of $J_{prod} > \langle J_{prod}\rangle + 1.5\Delta J_{prod}$ are deemed to correspond to residues with exchange.

A summary of the measured relaxation rates is shown in Table 1 and plotted in parts a−d of Figures 3. High average values for NOEs indicate that, except for the extreme N and C termini and parts of the RT loop, both the free and complexed p67^{phox}SH3(C) are reasonably well-ordered.

Calculation of the Hydrodynamic Parameters. In calculation of the overall hydrodynamic parameters for free p67^{phox}SH3(C), those residues that had NOE values < 0.6 were excluded (nine residues: 456, 457, 459, 462, 491, 496, 513, 515, and 516). Additionally, those residues with Δ_i values > 0.3 ppm (nine residues: 467, 468, 471, 472, 474, 479, 493, 505, and 509) and residues that included the mutation sites as well as one preceding residue and one following residue (four additional residues: 498, 499, 500, and 514) were excluded. An analysis using eq 8 to determine the residues undergoing conformational exchange above produced one additional residue, Val490. Thus, a total of 36 residues were used (two residues were Pro) to determine the rotational diffusion tensor. Calculations were performed using the ensemble of 22 NMR structures of the p67^{phox}SH3(C)/Pf complex (1K4U) (*11*). In the complex, 12 residues were excluded based on NOE < 0.6 (seven residues: 456, 457, 458, 460, 513, 515, and 516) and J_{prod} values (five residues: 459, 460, 462, 494, and 505). Thus, a total of 47 residues were utilized to calculate the overall rotational diffusion tensor. The J_{prod} for the two species are plotted in Figure 4.

Isotropic rotational diffusion tensors were obtained in both cases with $D_{xx} = D_{yy} = D_{zz} = D_{iso}$ values of 3.7 ± 0.1 ×

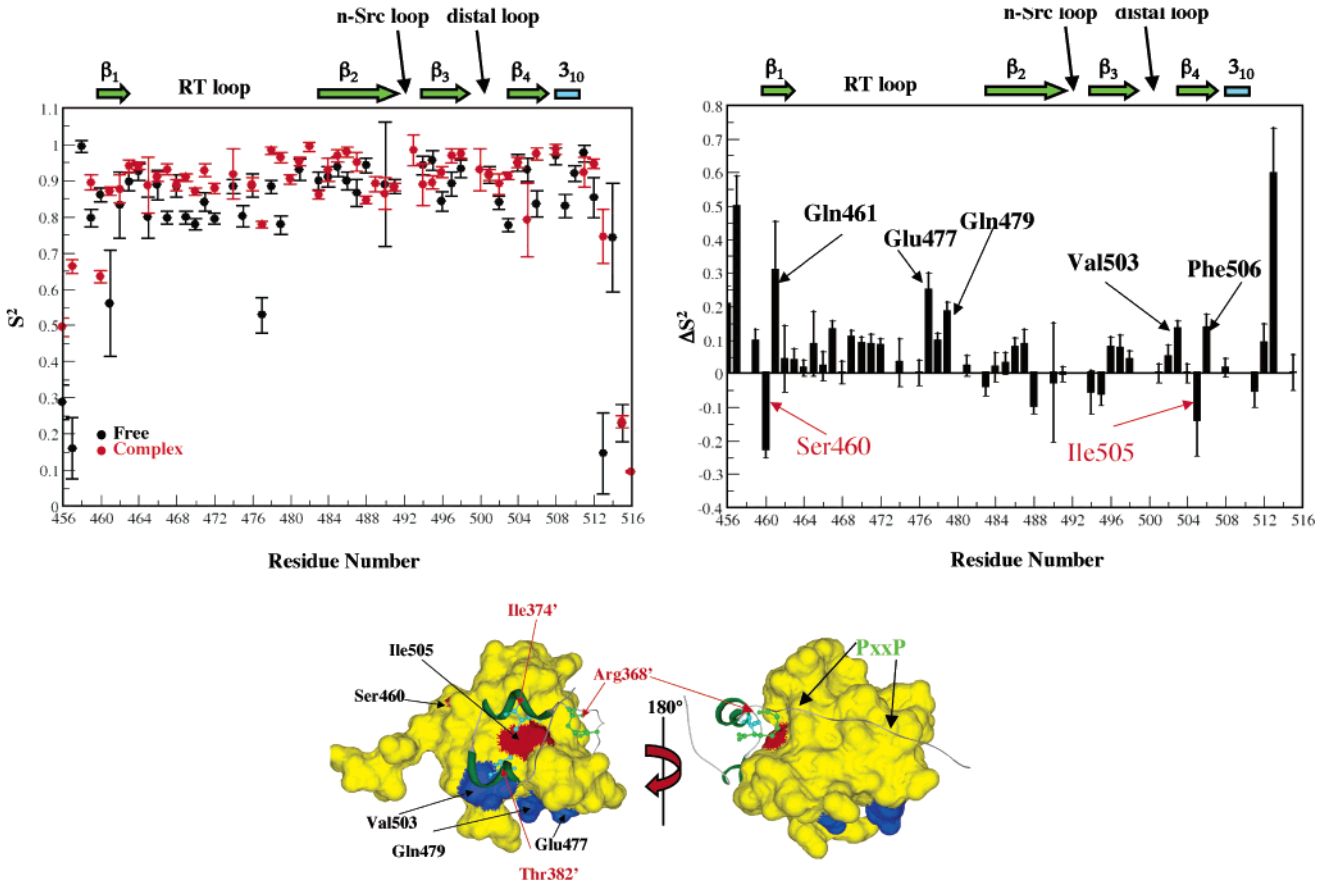

FIGURE 5: (a) Plot of S^2 for the free p67^{phox}SH3(C) (black) and the p67^{phox}SH3(C)/Pf complex (red). (b) Change in S^2 values upon complex formation. $\Delta S^2 = S^2$(complex) − S^2(free). Selected residues with large changes in S^2 values are labeled. Those residues that become more rigid on complex formation are labeled in black, while those that become more dynamic on complex formation are labeled in red. Ile505 plays a key role in the recognition of Pf by p67^{phox}SH3(C). (c) Residues that have $\Delta S^2 > 0.14$ are depicted in blue, and those with $\Delta S^2 < -0.14$ are shown in red on the p67^{phox}SH3(C) surface. Also shown are Ile374′ and Thr382′ (in cyan) and Arg368′ (in green) residues on Pf. Key residues on both p67^{phox}SH3(C) and Pf are labeled in black and red, respectively. The position of the PxxP motif (green labels) is shown schematically. Note, Arg368′ forms a part of the PxxPxR motif.

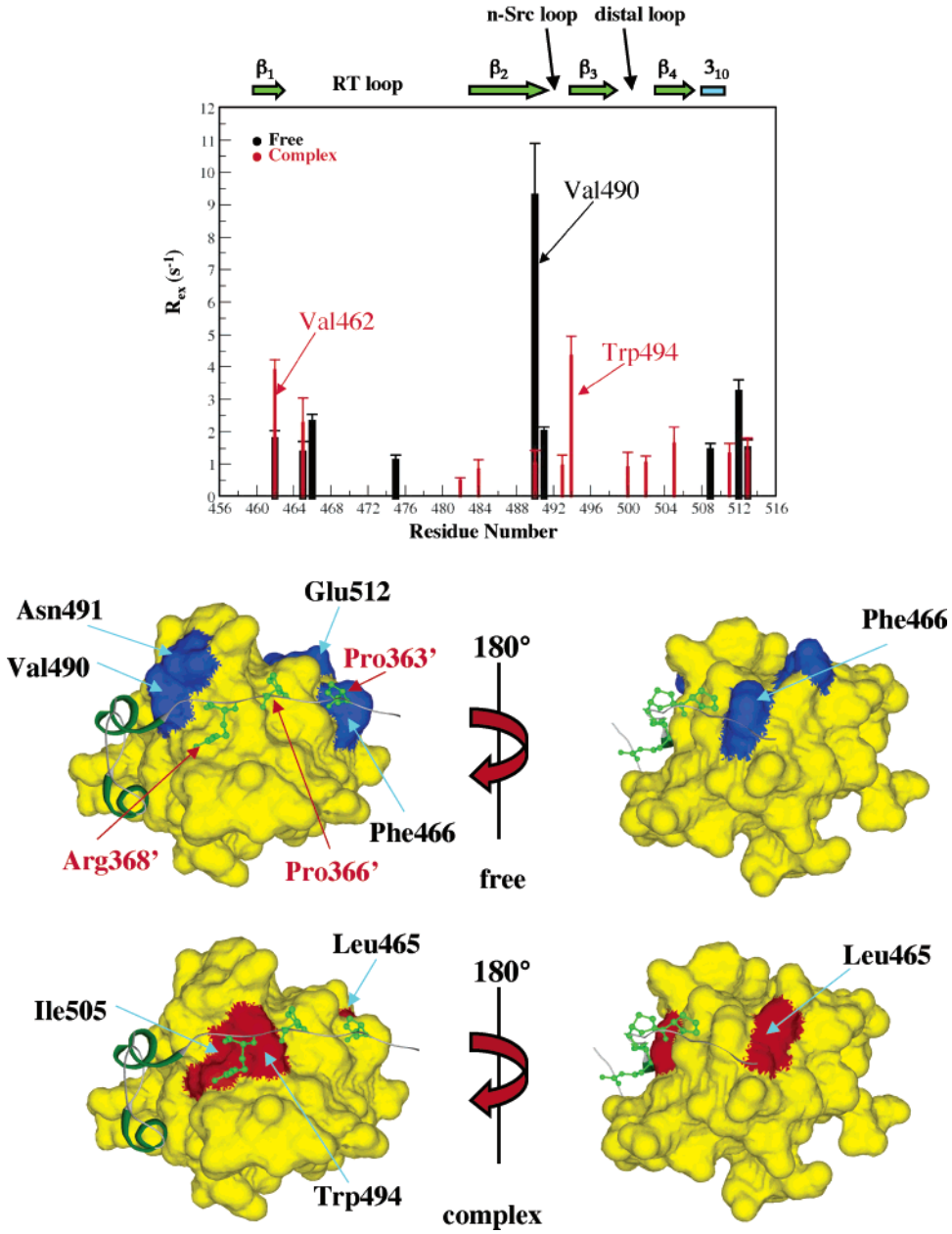

FIGURE 6: (a) Residues for the free (black) and complexed (red) p67^{phox}SH3(C) that yield R_{ex} values in the Lipari−Szabo analysis are shown. Residues with R_{ex} values >3.5 s^{-1} are labeled. (b) Residues with significant R_{ex} values (>1.5 s^{-1}) are shown on the surface of free (top, blue) and complexed (bottom, red) p67^{phox}SH3(C).

10^7 s^{-1} (τ_c = 4.5 ns) and 2.3 ± 0.1 × 10^7 s^{-1} (τ_c = 7.3 ns) for the free and complexed SH3 domains, respectively. These values were adjusted to 4.46 and 7.14 ns in the Lipari−Szabo approach described below to minimize the χ^2 value defined in eq 9.

Fast Motions on the Pico- to Nanosecond Time Scale. Analysis of the relaxation rates using the Lipari−Szabo approach revealed that backbone motion on the pico- to nanosecond time scale registered a small but significant decrease on complex formation in the p67^{phox}SH3(C) domain. The dynamic heterogeneity on this time scale also decreased upon complex formation. The average order parameters for the free and complexed p67^{phox}SH3(C) domains were found to be 0.81 ± 0.2 and 0.86 ± 0.17, respectively. The results are plotted in Figure 5a. The net changes in S^2 values on complex formation are shown in Figure 5b. It is seen that the largest changes ($|\Delta S^2| > 0.14$) were seen at the N and C terminus. Large positive changes (more rigid on complex formation) were also seen at the end of the RT loop. However, of greatest interest were the changes seen in the several residues that form the surface responsible for the specific recognition of the Pf peptide. These include large positive changes in Val503 (0.14 ± 0.02) and Phe506 (0.14 ± 0.04) and a large negative change (−0.14 ± 0.11) in Ile505. It is noteworthy that Ile505 through its δ_1 and γ_2 methyl groups makes key contacts with the δ_1 methyl of Ile374′ and γ_2 methyl of Thr382′ on Pf, thus conferring specificity to the p67^{phox}SH3(C)/Pf interaction. It is to be noted that I374′A and T382′A mutations reduce the binding affinity of Pf toward p67^{phox}SH3(C) 125- and 46-fold, respectively, indicating that the specific methyl−methyl interactions are key in stabilizing the complex. This behavior is reminiscent of the behavior of the residues that formed the specificity surface in the Csk-SH3/PEP-3BP1 interaction

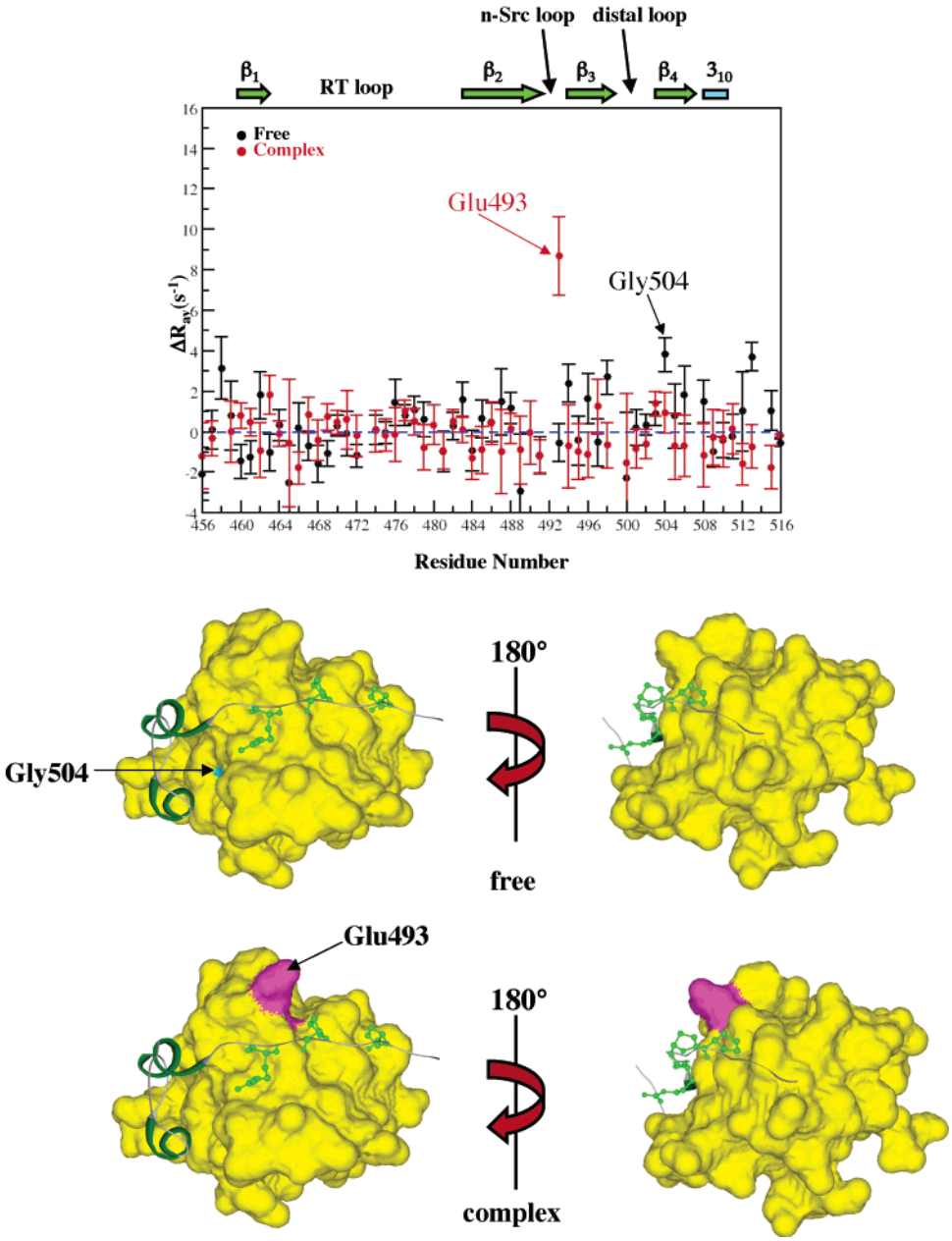

FIGURE 7: (a) $\Delta R_{av} = \Delta R_{av}(\tau_{CP} = 10\ ms) - \Delta R_{av}(\tau_{CP} = 1\ ms)$ are shown for the free (black) and complexed (red) p67^{phox}SH3(C). Selected residues with large ΔR_{av} values are labeled for the two species. The dashed line indicates $\Delta R_{av} = 0$ (b) Residues with significant ΔR_{av} values ($>2.0\ s^{-1}$) for the free (top, cyan) and complexed (bottom, pink) p67^{phox}SH3(C) are shown.

(vide infra). The fact that Ile505 does indeed become more disordered in complex formation and the negative ΔS^2 value obtained was not a mere artifact of the analysis was reconfirmed by using various subsets of the relaxation rates in the analysis, which consistently produced $\Delta S^2 < 0$. It was also seen that the C′−C$^{\alpha}$ bond vector for Ile505 with $S^2_{C'C\alpha} = 0.64$ was more disordered than the rest of the backbone ($\langle S^2_{C'C\alpha}\rangle = 0.83$; data not shown). In fact, it is notable that on complex formation Ile505 becomes disordered on multiple time scales exhibiting a slow local motion comparable to the overall correlation time ($\tau_{local} = 1.8$ ns) and showing a small R_{ex} value $= 1.6 \pm 0.5\ s^{-1}$. There is no detectable motion on either the nanosecond or the micro- to millisecond time scale in free p67^{phox}SH3(C). Further, it has been noted that as the local correlation time approaches the overall rotational correlation time of the Lipari−Szabo approach leads to an overestimation in order parameters (*24*). It is thus likely that the order parameter has actually been *overestimated* in the case of Ile505 in the complex and not in free p67^{phox}SH3(C), where no such motion exists. The key residues that show a significant change in S^2 values are mapped on to the p67^{phox}SH3(C) surface in Figure 5c. Residues at the end of the β strand (β_2) extending through the n-Src loop into the beginning of the third β strand (β_3) also displayed some increase in mobility upon complex formation. This could be due to a slight weakening of the interstrand interactions between β_2 and β_3 upon interactions with Pf in the complex.

Slow Motions on the Micro- to Millisecond Time Scale. Five residues in free p67^{phox}SH3(C) showed significant R_{ex} ($>1.5\ s^{-1}$) in the Lipari−Szabo analysis (Figure 6a). In the free SH3 domain, the largest R_{ex} value was seen in Val490 ($9.2 \pm 1.6\ s^{-1}$). Note that Val490 has a contact factor, $\Lambda_i = 0.894$, making stabilizing contacts with several residues

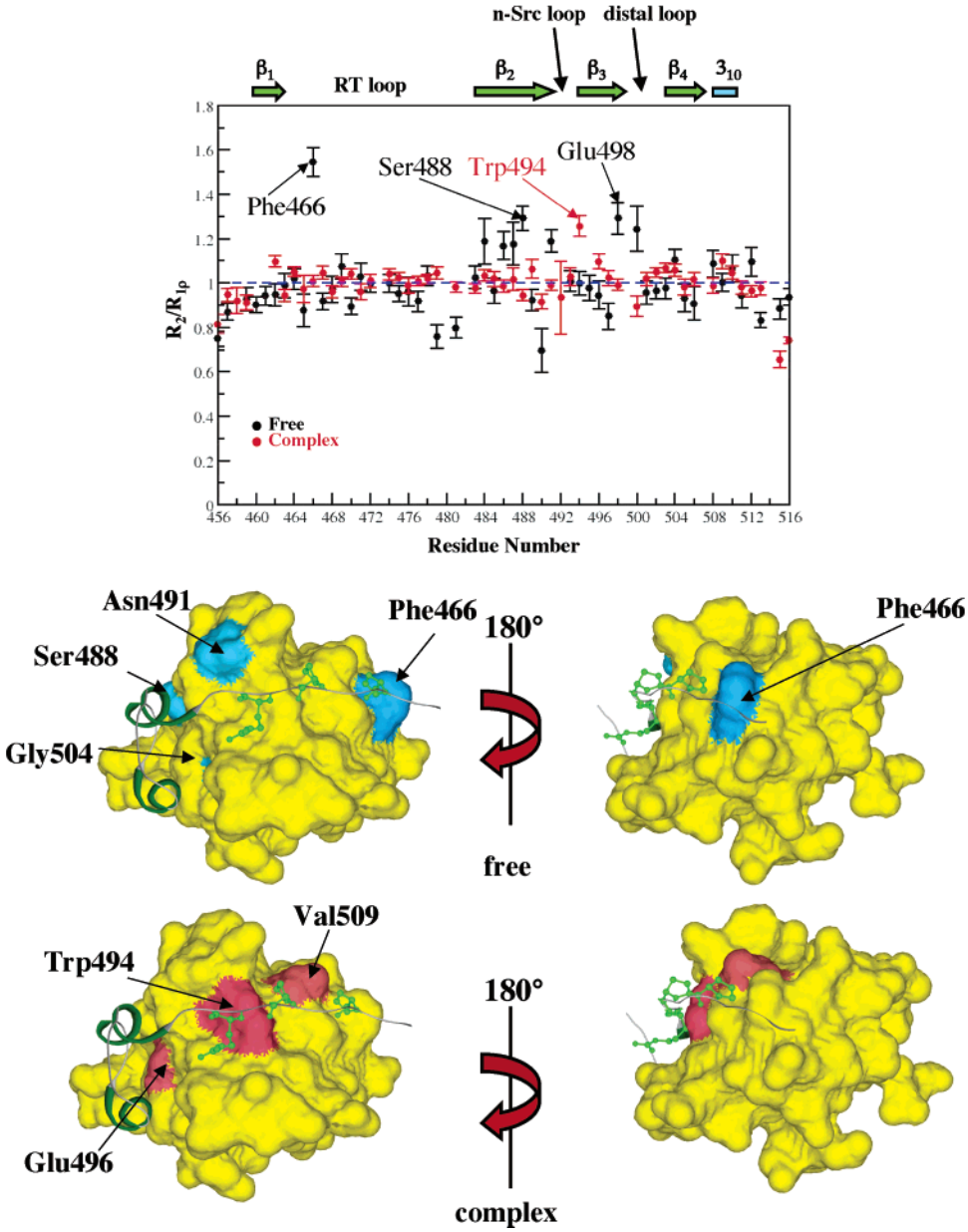

FIGURE 8: (a) Values of the $R_2/R_{1\rho}$ ratio for the free (black) and complexed (red) p67^{phox}SH3(C). The dashed line represents a $R_2/R_{1\rho} = 1$. Residues with $R_2/R_{1\rho} > 1.3$ are labeled. (b) Residues with $R_2/R_{1\rho} > 1.1$ for the free (top, blue) and complexed (bottom, pink) p67^{phox}SH3-(C) are shown.

corresponding to the C-terminal extension of the PxxP motif in Pf including Ile374′. The neighboring Asn491 (Λ_i = 0.884), which also makes several stabilizing contacts with Ile374′, also showed a significant R_{ex} value (1.9 ± 0.2 s^{-1}). Phe466 (Λ_i = 1.0) that makes several stabilizing contacts with Pro363′ of the PxxP motif of Pf shows a R_{ex} value of 2.3 ± 0.3 s^{-1}. In addition, significant R_{ex} values were seen in Val462 (1.7 ± 0.3 s^{-1}) and in the C-terminal Glu512 (3.2 ± 0.4 s^{-1}). In the complex, four residues showed significant R_{ex} values, these included Val462 (3.9 ± 0.3 s^{-1}), Leu465 (2.3 ± 0.7 s^{-1}), Trp494 (4.3 ± 0.6 s^{-1}), and Ile505 (1.6 ± 0.5 s^{-1}). Leu465 and Trp494 recognize key residues of the PxxPxR motif with the former lying next to Phe466 that recognizes Pro363′ (see above) and the latter making stabilizing contacts with Arg368′ (which forms a part of the PxxPxR motif that defines the orientation of a class II ligand). Ile505 is key in the specific recognition of Pf by p67^{phox}-SH3(C). These residues for both the free and complexed state are mapped on the surface of p67^{phox}SH3(C) in Figure 6b.

We also investigated dynamic processes in the 1−10 ms time scale. The conventional CPMG-based R_2 rates used in the Lipari−Szabo analysis discussed above are insensitive to this time scale because of the rapid repetition rate of the π pulses (1 ms) of the CPMG cycle used to measure the R_2 values. We employed the RC-CPMG sequence of Loria et al. (*18*) using τ_{CP} values of 1 and 10 ms (Figure 7a). $\Delta R_{av} = R_{av}(\tau_{CP} = 10\text{ ms}) - R_{av}(\tau_{CP} = 1\text{ ms})$ values >2.0 s^{-1} were assumed to indicate slow motion in the 1−10 ms time scale. Using this criterion, Gly504 (3.8 ± 0.8 s^{-1}) in the free SH3 domain and Glu493 (8.7 ± 1.9 s^{-1}) in the complex were deemed to display dynamics in the 1−10 ms time scale. Gly504 has a Λ_i value of 0.874 and makes stabilizing contacts with Thr382′, which is, as stated previously, a key residue in defining the specificity of the p67^{phox}SH3(C)/Pf interaction. Glu493 (Λ_i = 0.725), on the other hand, lies

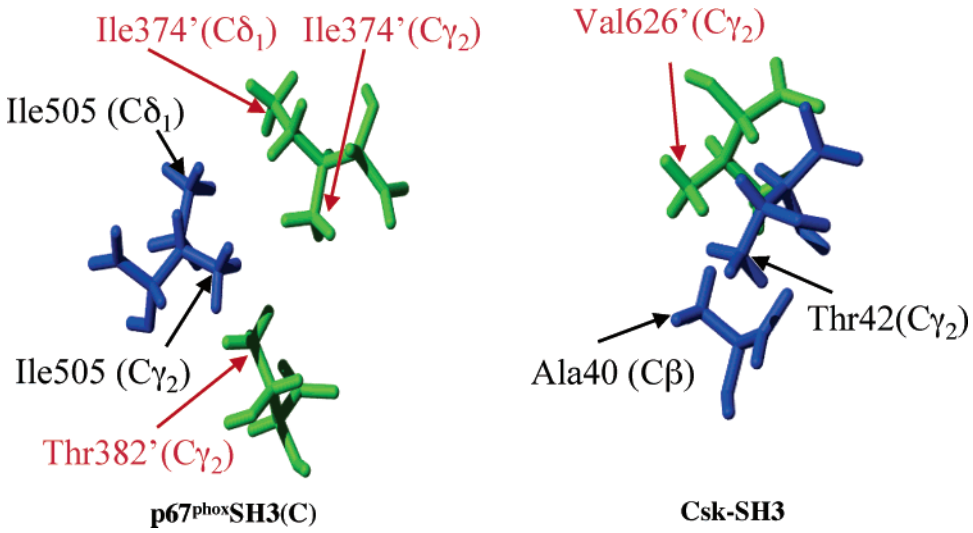

FIGURE 9: Detailed comparison of the interactions that determine the specificity in the p67^{phox}SH3(C)/Pf (left) and Csk-SH3/PEP-3BP1 (right) interactions. Notably, the $^1H^N$ vector of Ile505 in p67^{phox}SH3(C) becomes more disordered on complex formation, and the $^1H^N$ vectors of Ala40 and Thr42 show S^2 values far lower than the mean in the Csk-SH3/3BP1 complex. The residues corresponding to the SH3 domains are shown in blue and labeled in black, while those corresponding to their respective ligands are shown in green and labeled in red.

close to Trp494, which, as stated above, is key in recognizing the PxxP motif. Glu493 itself contacts Pro366′. Key residues are indicated in Figure 7b.

A comparison of the corrected $R_{1\rho}$ and R_2 values provides information about motion on the submillisecond time scale. In the fast exchange limit, for a two-site exchange, the ratio $R_2/R_{1\rho}$ may be expressed as

$$\frac{R_2}{R_{1\rho}} = \frac{R_2^0 + p_A p_B \Delta\omega^2 \tau_{ex}}{R_2^0 + p_A p_B \Delta\omega^2 \left(\dfrac{\tau_{ex}}{1 + \omega_{SL}{}^2 \tau_{ex}{}^2}\right)} \qquad (10)$$

R_2^0 is the rate in the absence of exchange, p_A and p_B are the populations of the two sites, $\Delta\omega$ is the difference in resonance frequency between the sites, and ω_{SL} is the strength of the spin-lock field. In the present case, the quantity $\omega_{SL}{}^2\tau_{ex}{}^2 \approx 90$ for $\tau_{ex} = 1$ ms and $R_2/R_{1\rho} > 1$. This ratio is equal to 1 in the absence of exchange. Note that eq 10 is valid in the limit $\tau_{CP} \ll \tau_{ex}$ (*25*). Further, it has been noted that off-resonance effects in CPMG-based sequences underestimate R_2 values (*26*), and conventional strategies (such as those employed here), to measure $R_{1\rho}$ values, overestimate them (*27*). In the present case, it is probable that $R_2/R_{1\rho}$ have been underestimated for certain residues. Thus, $R_2/R_{1\rho}$ values greater than 1 (Figure 8a) are indicative of the presence of motions in the hundreds of microseconds regime. In the present case, values of the ratio >1.1 are considered significant. For the free SH3 domain, the residue with the largest $R_2/R_{1\rho}$ ratio was Phe466 (1.55 ± 0.07). Phe466 (Λ_i = 1.0) makes multiple stabilizing contacts with Pro363′. In addition, Ser488 (1.3 ± 0.06) shows a large deviation from 1 and lies close to Val490, which makes several contacts with Ile374′ on Pf. In the complex, the largest value was shown by Trp494 (1.3 ± 0.05) that as mentioned before is one of the key residues in the PxxP motif recognition. Key residues that display motion on the submillisecond time scale for both free and complexed p67^{phox}SH3(C) are depicted in Figure 8b.

DISCUSSION

Analysis of the dynamics of p67^{phox}SH3(C) in the free state and in complex with Pf reveals the following features: for the fast (pico- to nanosecond) time scale motions, residues near the specificity site show large changes in dynamics upon complex formation. Notably, Ile505, which makes several contacts with the two key residues (Ile374′ and Thr382′) on Pf that define the high affinity and high specificity of the interaction, and becomes less rigid upon complex formation. In the micro- to millisecond time scale, significant motion exists in and near residues on the SH3 domain responsible both for the canonical PxxP recognition and the specificity surfaces. However, significant motion on this time scale exists only in and near residues forming the PxxP recognition surface in the complex. However, Ile505, which plays a central role in specific recognition of Pf does show a small but significant R_{ex} term on complex formation, seemingly becoming more disordered on multiple time scales.

As mentioned above for Ile505 on p67^{phox}SH3(C), the γ_2 methyl group interacts with the γ_2 methyl group of Thr382′ and the δ_1 methyl group interacts with δ_1 methyl group of Ile374′ on Pf. These interactions provide high specificity to the p67^{phox}SH3(C)/Pf interaction. An inspection of the cluster of 22 structures of the complex (1K4U) reveals that the average side chain torsion angles χ_1 (41.5 ± 1.8) and χ_{21} (145.0 ± 6.6) are very well-ordered for Ile505. This is in complete contrast to the backbone NH vector that becomes more disordered on complex formation, as shown by the present analysis of dynamics. This parallels the effect seen in the specificity surface for Csk-SH3 (see Figure 9). In the case of Csk, the β methyl group of Ala40 and the γ_2 methyl group of Thr42 on Csk-SH3 interact with the γ_2 methyl group of Val626′ on PEP-3BP1. This interaction is key to yielding the high affinity and specificity to the Csk-SH3/PEP-3BP1 interaction. An analysis of the backbone dynamics of the Csk-SH3/PEP-3BP1 complex (*10*) revealed that the order parameters for the backbone amide vector for Ala40 (0.36) and Thr42 (0.68) were far lower than the average for the ordered parts of the backbone (0.86) and the {^{15}N-$^1H^N$}-NOE

Table 2: Relation with Conservation and Micro- to Millisecond Time Scale Motion in the Csk-SH3/PEP-3BP1, Free p67^{phox}SH3(C), and p67^{phox}SH3(C)/Pf Complex[a]

residue	consensus	rates (s^{-1}) or $R_2/R_{1\rho}$ ratio	positional entropy	role
		Csk-SH3/PEP-3BP1		
Ile59[b]	Leu49	13.1 ± 4.7	8.6	binding
Gly58[b]	**Gly48**	**11.9 ± 1.6**	**1.4**	**structural**
Tyr48[b]	Trp37	10.6 ± 3.3	4.7	core
Ile60[b]	Phe50	8.9 ± 3.6	4.5	core
Asp44[b]		8.7 ± 1.7		
Ala52[b]		8.0 ± 3.8		
Trp47[b]	**Trp36**	**6.3 ± 0.9**	**1.3**	**binding**
Ala50[b]	Gly39	6.2 ± 1.2	3.8	core
Asp27[b]	Glu17	4.9 ± 0.7	5.2	RT
		p67^{phox}SH3(C) Free		
Gly504[b]	**Gly48**	**3.8 ± 0.8**	**1.4**	**structural**
Val490[c]		9.2 ± 1.6		
Glu512[c]		3.2 ± 0.4		
Phe466[c,d]	Tyr10	2.3 ± 0.3	3.4	binding
Asn491[c]	Asp33	1.9 ± 0.2	8.4	binding
Val462[c]	Arg5	1.7 ± 0.3	7.6	not known
Ala488[e]		1.30 ± 0.05		
Val486[e]	Val28	1.17 ± 0.07	3.9	core
Glu492[f]				
		p67^{phox}SH3(C)/Pf Complex		
Glu493[b]	Gly35	8.7 ± 1.9	7.3	binding
Trp494[c]	**Trp36**	**4.3 ± 0.6**	**1.3**	**binding**
Val462[c]	Arg5	3.9 ± 0.3	7.6	not known
Leu465[c]	Leu7	2.3 ± 0.8	6.1	structural
Ile505[c]	Leu49	1.6 ± 0.5	8.6	binding
Glu496[e]		1.1 ± 0.03		
Val509[e]	Asn53	1.1 ± 0.03	6.5	binding
Glu492[f]				

[a] Some residues show micro- to millisecond time scale motions from multiple measurements; these are not duplicated in the table. Positional entropy values are the same as in Larson and Davidson (*28*). [b] $\Delta R_{av} = \Delta R_{av}(\tau_{CP} = 10\ ms) - \Delta R_{av}(\tau_{CP} = 1\ ms) > 2.0\ s^{-1}$. [c] R_{ex} values > 1.5 s^{-1}. [d] Largest $R_2/R_{1\rho}$ value = 1.55 ± 0.07. [e] $R_2/R_{1\rho}$ values > 1.1. [f] Too broad for accurate analysis in both free and complexed forms.

value for Val626′ (0.37) was also far lower than the average (0.72). This dynamic effect is seen to be extremely local to the key specificity site both in the case of p67^{phox}SH3(C) and Csk-SH3. A plausible explanation of this phenomenon may be found in the fact that the ability to freely rotate about certain side-chain dihedral angles (χ_1 and χ_2 in Ile505) is lost upon complex formation and this loss in side-chain conformational entropy may be partially compensated by increased local mobility in the protein backbone in the complex. A clearer view of this phenomenon can be obtained from the study of side-chain dynamics in the free and complexed states.

It has been seen above that the regions in which the largest extent of motion in the micro- to millisecond time scale persist in the complex constitute residues that are key in recognizing the canonical PxxPxR motif (class II SH3 ligand). This was also the case seen in the Csk-SH3/PEP-3BP1 complex. Since several of the residues that define this surface are highly conserved in SH3 domains, we investigated the conservation of those residues that exhibit motion on the slow time scale in free p67^{phox}SH3(C), in the p67^{phox}SH3(C)/Pf complex, and in the Csk-SH3/PEP-3BP1 complex. These results are summarized in Table 2. A large majority of the residues that exhibit motion in the micro- to millisecond time scale belong to the 30 most conserved positions in SH3 domains (*28*). The consensus numbering scheme used is that defined by Larson and Davidson (*28*). Table 2 reveals that two residues (using the consensus numbering scheme) Gly48 (Gly504 in p67 and Gly58 in Csk) and Trp36 (Trp494 in p67 and Trp47 in Csk) in addition to residues flanking them display a substantial mobility in the micro- to millisecond time scale. Gly48 (entropy = 1.4) and Trp36 (entropy = 1.3) are almost completely conserved in SH3 domains. Trp36 is a key binding residue and its indole H^{ϵ} is often involved in hydrogen-bond formation with the backbone C′ of the second proline in the PxxP motif. Notably, the $N^{\epsilon}H^{\epsilon}$ vector showed no mobility on the slow time scale either in free or complexed p67^{phox}SH3(C) or in the Csk-SH3/PEP-3BP1 complex. The role of Gly48 is not clear, though mutations at this position result in a greatly decreased stability (*28*). The extent of slow motion seen in the residues corresponding to the consensus Gly48 is comparatively (compared to other residues in the same system) large both in free p67^{phox}SH3(C) (Gly504, ΔR_{av} = 3.8) and in the Csk-SH3/PEP-3BP1 complex (Gly58, ΔR_{av} = 11.9). However, there is no significant dynamics on this time scale in the p67^{phox}SH3(C)/Pf complex for this residue. This is hardly surprising because this residue lies close to Ile505 that forms a part of the specificity surface. It does however show a $R_2/R_{1\rho}$ value of 1.06 that may be indicative of some residual slow motion. As previously noted, Ile505 does show a small but significant R_{ex} value (1.6 s^{-1}) upon complex formation. The corresponding residue in Csk-SH3 is Ile59 (the consensus residue in SH3 domains being Leu49, entropy = 8.6), which displays the largest ΔR_{av} value (13.1 s^{-1}). This observation indicates that this region in the complexed state has a tendency to exhibit micro- to millisecond time scale motion, but this is significantly suppressed by the presence of the specific interaction involving Ile505 in the case of p67^{phox}SH3(C). A comparison of the surfaces that exhibit micro- to millisecond time scale motion in p67^{phox}SH3(C) and Csk-SH3 complexed with Pf and PEP-3BP1, respectively, are shown in Figure 10. The general shape of the two surfaces is quite similar. The $R_{1\rho}$ data are not available for the Csk-SH3/PEP-3BP1 complex (note that, in p67^{phox}SH3(C), slow motion in Glu496 and Val509 was detected using the $R_2/R_{1\rho}$ ratio).

A question remains on the origin of these slow motions seen in the complexed states both in Csk-SH3 and in p67^{phox}-SH3(C). The regions where these motions are the most significant are concentrated essentially in the n-Src (extending into β_3) and distal loops (extending into β_4). It has been shown that these regions possess extremely large values for the free energy of HD exchange in Src-SH3 (ΔG_{HD}), and these values also have the largest dependence on the concentration of denaturant (*29*). It is thus unlikely that these slow motions arise from local unfolding events because this would lead to instability in the β-sandwich structure of the SH3 domain (*29*). It may therefore be conjectured that these motions arise from the reorganization of key residues in the SH3 domain and the corresponding conformational reorganization of the peptide residues. Thus, in an ensemble sense, it may be assumed that several conformers of slightly different structure of the protein exist at any given time. These conformers are situated in local minima not too far in energy from the global minimum separated by barriers comparable to the thermal energy. This makes the landscape about the global minimum quite rugged. Each of these

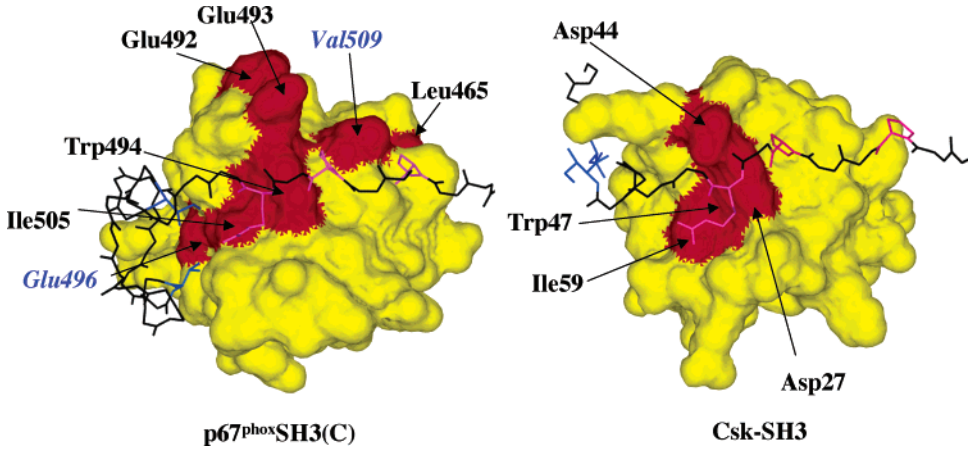

FIGURE 10: Comparison of the surfaces that display motion on the micro- to millisecond time scale in the p67^{phox}SH3(C)/Pf (left) and Csk-SH3/PEP-3BP1 (right) complexes. Key residues are labeled in both cases. The residues in p67^{phox}SH3(C), where the slow motion was detected using elevated values of the $R_2/R_{1\rho}$ ratio, are italicized and labeled in blue. The $R_{1\rho}$ rates are not available for Csk-SH3.

conformers are capable of accommodating ligands of slightly different structures as long as gross structural features are present, resulting in nonspecific binding (*30*, *31*). Thus, the micro- to millisecond time scale motions may be considered to be conformational transitions across the thermally surmountable barriers and corresponding conformational transitions in the ligand (in the PxxPxR motif). Thus, if this were true, one would expect to see dynamics on similar time scales in the PxxPxR motif on the ligand. In the case of PEP-3BP1, it was noted that Leu616′, which was in the center of the PxxP (PPLP) motif, showed the largest ΔR_{av} value (*10*). Thus, the presence of slow motions may be considered to be signatures of nonspecifically binding surfaces such the proline-helix recognition surface in SH3 domains.

Despite the similarities seen between Csk-SH3 and p67^{phox}-SH3(C), a major difference is the fact that there does not seem to be a clear separation of dynamic time scales between the proline-helix recognition surface and the specificity surface in p67^{phox}SH3(C) as in Csk-SH3. It has been stated above that Ile505, which is key in defining the specificity of the p67^{phox}SH3(C)/Pf interaction, does show a small but significant R_{ex} term upon complex formation. In Csk-SH3, on the other hand, the residues forming the specificity surface were dynamic on the fast, pico- to nanosecond time scale, and those of the proline-helix recognition surface were dynamic on the micro- to millisecond time scale. This is hardly surprising because the common area shared by the two surfaces is significantly larger in p67^{phox}SH3(C) than in Csk-SH3 as shown in Figure 1. Thus, it is expected that the dynamical coupling between the two surfaces would be larger in p67^{phox}SH3(C) than in Csk-SH3.

In conclusion, we have studied the backbone dynamics of the C-terminal SH3 domain of p67^{phox} in complex with a 32-residue peptide from the proline-rich tail of p47^{phox}. Several dynamic changes are seen on complex formation both on the fast (pico- to nanosecond) and the slow (micro- to millisecond) time scale. Ile505, responsible for providing key contacts that determine the specificity of the p67^{phox}/p47^{phox} interaction, becomes disordered on multiple time scales upon complex formation. This is probably in part to compensate for the loss in side-chain entropy upon complex formation. The micro- to millisecond motions that persist in the complex involve several residues that are involved in the canonical PxxP motif recognition and are highly conserved in SH3 domains. The general nature of the slow dynamics seen in the p67^{phox}SH3(C)/Pf complex is quite similar to that seen in the Csk-SH3/PEP-3BP1 complex. The slow dynamics are indicative of transitions between conformers of slightly different structures separated by energy barriers of the order of the thermal energy and are indicative of nonspecific recognition surfaces and ruggedness about the global minimum. The studies here have been limited to backbone dynamics, though a large majority of the protein−ligand interactions in SH3 domains occur through the side chains. Thus, a clearer understanding of the dynamic properties of SH3 domains can be obtained by a detailed analysis of side-chain dynamics (*32*, *33*). Further, it is expected that the canonical PxxP motif recognition surface exhibits medium- and long-range correlated motions on the slow time scale. We are in the process of applying recently proposed methods (*34*) to investigate the role of correlated motions in proline-helix recognition by SH3 domains.

ACKNOWLEDGMENT

The authors thank Prof. Hideki Sumimoto (Department of Biochemistry and Molecular Biology, Medical Institute of Bioregulation) and Prof. Daisuke Kohda (Department of Structural Biology, Medical Institute of Bioregulation) at Kyushu University for useful discussions. The authors also thank Prof. Arthur G. Palmer, III of Columbia University and Dr. David Cowburn at the New York Structural Biology Center for insightful discussions on the interpretation of the relaxation rates.

REFERENCES

1. Morton, C. J., and Campbell, I. D. (1994) SH3 domains. Molecular "Velcro", *Curr. Biol. 4*, 615−617.
2. Mayer, B. J. (2001) SH3 domains: Complexity in moderation, *J. Cell Sci. 114*, 1253−1263.
3. Mayer, B., and Baltimore, D. (1993) Signaling through SH2 and SH3 domains, *Trends Cell Biol. 3*, 8−13.
4. Pawson, T. (1994) SH2 and SH3 domains in signal transduction, *Adv. Cancer Res. 64*, 87−110.
5. Yu, H., Chen, J. K., Feng, S., Dalgarno, D. C., Brauer, A. W., and Schreiber, S. L. (1994) Structural basis for the binding of proline-rich peptides to SH3 domains, *Cell 76*, 933−945.
6. Lim, W. A., Richards, F. M., and Fox, R. O. (1994) Structural determinants of peptide-binding orientation and of sequence specificity in SH3 domains, *Nature 372*, 375−379.

7. Gregorieff, A., Cloutier, J. F., and Veillette, A. (1998) Sequence requirements for association of protein-tyrosine phosphatase PEP with the Src homology 3 domain of inhibitory tyrosine protein kinase $p50^{csk}$, *J. Biol. Chem. 273*, 13217−13222.
8. Courtneidge, S. A., Fumagalli, S., Koegl, M., Superti-Furga, G., and Twamley-Stein, G. M. (1993) The Src family of protein tyrosine kinases: Regulation and functions, *EMBO J.* 57−64.
9. Williams, J. C., Wierenga, R. K., and Saraste, M. (1998) Insights into Src kinase functions: Structural comparisons, *Trends Biochem. Sci. 23*, 179−184.
10. Ghose, R., Shekhtman, A., Goger, M. J., Ji, H., and Cowburn, D. (2001) A novel, specific interaction involving the Csk SH3 domain and its natural ligand, *Nat. Struct. Biol. 8*, 998−1004.
11. Kami, K., Takeya, R., Sumimoto, H., and Kohda, D. (2002) Diverse recognition of non-PxxP peptide ligands by the SH3 domains from $p67^{phox}$, Grb2, and Pex13p, *EMBO J. 21*, 4268−4276.
12. Cesareni, G., Panni, S., Nardelli, G., and Castagnoli, L. (2002) Can we infer peptide recognition specificity mediated by SH3 domains? *FEBS Lett. 513*, 38−44.
13. Wang, C., Pawley, N. H., and Nicholson, L. K. (2001) The role of backbone motions in ligand binding to the c-Src SH3 domain, *J. Mol. Biol. 313*, 873−887.
14. Ferreon, J. C., and Hilser, V. J. (2003) Ligand-induced changes in dynamics in the RT loop of the C-terminal SH3 domain of Sem-5 indicate cooperative conformational coupling, *Protein Sci. 12*, 982−996.
15. Kay, L. E., Muhandiram, D. R., Farrow, N. A., Aubin, Y., and Forman-Kay, J. D. (1996) Correlation between dynamics and high affinity binding in an SH2 domain interaction, *Biochemistry 35*, 361−368.
16. Vaughn, J. L., Feher, V. A., Bracken, C., and Cavanagh, J. (2001) The DNA-binding domain in the *Bacillus subtilis* transition-state regulator AbrB employs significant motion for promiscuous DNA recognition, *J. Mol. Biol. 305*, 429−439.
17. Palmer, A. G., III (2001) NMR probes of molecular dynamics: Overview and comparison with other techniques, *Annu. Rev. Biophys. Biomol. Struct. 30*, 129−155.
18. Loria, J. P., Rance, M., and Palmer, A. G. I. (1999) A relaxation-compensated Carr−Purcell−Meiboom−Gill sequence for characterizing chemical exchange by NMR spectroscopy, *J. Am. Chem. Soc. 121*, 2331−2332.
19. Delaglio, F., Grzesiek, S., Vuister, G. W., Zhu, G., Pfeifer, J., and Bax, A. (1995) NMRPipe: A multidimensional spectral processing system based on UNIX pipes, *J. Biomol. NMR 6*, 277−293.
20. Ghose, R., Fushman, D., and Cowburn, D. (2001) Determination of the rotational diffusion tensor of macromolecules in solution from NMR relaxation data with a combination of exact and approximate methods−Application to the determination of interdomain orientation in multidomain proteins, *J. Magn. Reson. 149*, 204−217.
21. Kneller, J. M., Lu, M., and Bracken, C. (2002) An effective method for the discrimination of motional anisotropy and chemical exchange, *J. Am. Chem. Soc. 124*, 1852−1853.
22. Lipari, G., and Szabo, A. (1982) Model-free approach to the interpretation of nuclear magnetic resonance relaxation in macromolecules. 1. Theory and range of validity, *J. Am. Chem. Soc. 104*, 4546−4559.
23. Fushman, D., Cahill, S., and Cowburn, D. (1997) The main chain dynamics of the dynamin pleckstrin homology (PH) domain in solution: Analysis of ^{15}N relaxation with monomer/dimer equilibration, *J. Mol. Biol. 266*, 173−194.
24. Tugarinov, V., Liang, Z., Shapiro, Y. E., Freed, J. H., and Meirovitch, E. (2001) A structural mode-coupling approach to ^{15}N NMR relaxation in proteins, *J. Am. Chem. Soc. 123*, 3055−3063.
25. Ishima, R., and Torchia, D. A. (1999) Estimating the time scale of chemical exchange of proteins from measurements of transverse relaxation rates in solution, *J. Biomol. NMR 14*, 369−372.
26. Korzhnev, D. M., Tischenko, E. V., and Arseniev, A. S. (2000) Off-resonance effects in ^{15}N T_2 CPMG measurements, *J. Biomol. NMR 17*, 231−237.
27. Korzhnev, D. M., Orekhov, V. Y., Dahlquist, F. W., and Kay, L. E. (2003) Off-resonance $R_{1\rho}$ relaxation outside of the fast exchange limit: An experimental study of a cavity mutant of T4 lysozyme, *J. Biomol. NMR 26*, 39−48.
28. Larson, S. M., and Davidson, A. R. (2000) The identification of conserved interactions within the SH3 domain by alignment of sequences and structures, *Protein Sci. 9*, 2170−2180.
29. Grantcharova, V. P., and Baker, D. (1997) Folding dynamics of the Src SH3 domain, *Biochemistry 36*, 15685−15692.
30. Ma, B., Kumar, S., Tsai, C. J., and Nussinov, R. (1999) Folding funnels and binding mechanisms, *Protein Eng. 12*, 713−720.
31. Ma, B., Shatsky, M., Wolfson, H. J., and Nussinov, R. (2002) Multiple diverse ligands binding at a single protein site: A matter of pre-existing populations, *Protein Sci. 11*, 184−197.
32. Yang, D., and Kay, L. (1996) The effect of cross correlation and cross relaxation on the measurement of deuterium T_1 and $T_{1\rho}$ relaxation times in $^{13}CH_2D$ spin systems, *J. Magn. Reson., Ser. B 110*, 213−218.
33. Millet, O., Muhandiram, D. R., Skrynnikov, N. R., and Kay, L. E. (2002) Deuterium spin probes of side-chain dynamics in proteins. 1. Measurement of five relaxation rates per deuteron in ^{13}C-labeled and fractionally ^{2}H-enriched proteins in solution, *J. Am. Chem. Soc. 124*, 6439−6448.
34. Majumdar, A., and Ghose, R. (2004) Probing slow backbone dynamics in proteins using TROSY-based experiments to detect cross-correlated time-modulation of isotropic chemical shifts, *J. Biomol. NMR 28*, 213−227.

BI030268D